ISSN 1674-1056
http://cpb.iphy.ac.cn
http://iopscience.iop.org/cpb
中国物理 B
Chinese Physics
中国物理 Chinese Physics B

## Possible nodeless $s^{\pm}$-wave superconductivity intwisted bilayer graphene

Zhe Liu(刘哲), Yu Li(李宇), Yi-feng Yang(杨义峰)

**Citation:**Chin. Phys. B . 2019, 28(7): 077103. **doi:** 10.1088/1674-1056/28/7/077103
Journal homepage: http://cpb.iphy.ac.cn; http://iopscience.iop.org/cpb

**What follows is a list of articles you may be interested in**

---

## Negative differential resistance and quantum oscillations in $FeSb_2$ with embedded antimony

Fangdong Tang(汤方栋), Qianheng Du(杜乾衡), Cedomir Petrovic, Wei Zhang(张威), Mingquan He(何明全), Liyuan Zhang(张立源)

Chin. Phys. B . 2019, 28(3): 037104. **doi:** 10.1088/1674-1056/28/3/037104

## Magnetochemistry and chemical synthesis

Lin Hu(胡林), Guoliang Xia(夏国良), Qianwang Chen(陈乾旺)

Chin. Phys. B . 2019, 28(3): 037102. **doi:** 10.1088/1674-1056/28/3/037102

## Heavy fermions in high magnetic fields

M Smidman, B Shen(沈斌), C Y Guo(郭春煜), L Jiao(焦琳), X Lu(路欣), H Q Yuan(袁辉球)

Chin. Phys. B . 2019, 28(1): 017106. **doi:** 10.1088/1674-1056/28/1/017106

## Pressure effect in the Kondo semimetal $CeRu_4Sn_6$ with nontrivial topology

Jiahao Zhang(张佳浩), Shuai Zhang(张帅), Ziheng Chen(陈子珩), Meng Lv(吕孟), Hengcan Zhao(赵恒灿), Yi-feng Yang(杨义峰), Genfu Chen(陈根富), Peijie Sun(孙培杰)

Chin. Phys. B . 2018, 27(9): 097103. **doi:** 10.1088/1674-1056/27/9/097103

## Voltage-controlled Kosterlitz-Thouless transitions and various kinds of Kondo behaviors in a triple dot device

Yong-Chen Xiong(熊永臣), Jun Zhang(张俊), Wang-Huai Zhou(周望怀), Amel Laref

Chin. Phys. B . 2017, 26(9): 097102. **doi:** 10.1088/1674-1056/26/9/097102

---

RAPID COMMUNICATION

# Possible nodeless $s^{\pm}$-wave superconductivity in twisted bilayer graphene*

Zhe Liu(刘哲)[1], Yu Li(李宇)[1,2], and Yi-Feng Yang(杨义峰)[1,2,3,4,†]

[1] *Beijing National Laboratory for Condensed Matter Physics and Institute of Physics, Chinese Academy of Sciences, Beijing* 100190, *China*
[2] *University of Chinese Academy of Sciences, Beijing* 100049, *China*
[3] *Songshan Lake Materials Laboratory, Dongguan* 523808, *China*
[4] *Collaborative Innovation Center of Quantum Matter, Beijing* 100190, *China*

(Received 6 May 2019; published online 31 May 2019)

The recent discovery of superconductivity in the twisted bilayer graphene has stimulated numerous theoretical proposals concerning its exact gap symmetry. Among them, the d + id or p + ip-wave was believed to be the most plausible solution. Here, considering that the superconductivity emerges near a correlated insulating state and may be induced by antiferromagnetic spin fluctuations, we apply the strong-coupling Eliashberg theory with both inter- and intraband quantum critical pairing interactions and discuss the possible gap symmetry in an effective low-energy four-orbital model. Our calculations reveal a nodeless $s^{\pm}$-wave as the most probable candidate for the superconducting gap symmetry in the experimentally relevant parameter range. This solution is distinctly different from previous theoretical proposals. It highlights the multi-gap nature of the superconductivity and puts the twisted bilayer graphene in the same class as the iron-pnictide, electron-doped cuprate, and some heavy fermion superconductors.

**Keywords:** twisted bilayer graphene, superconductivity

**PACS:** 71.27.+a, 74.70.Tx **DOI:** 10.1088/1674-1056/28/7/077103

The recent discovery of superconductivity in twisted bilayer graphene (TBLG) has attracted tremendous interest[1,2] in the condensed matter community. Depending on the twisted angle, TBLG can exhibit a large variety of exotic phenomena.[3–30] For a small twisted angle, as shown in Fig. 1(a), the lattice can form the so-called Moiré superlattice[28–32] with strongly renormalized low-energy Dirac fermions.[20–28] At the so-called "magic angles", their Fermi velocity can even be reduced to zero.[26–29] The superconducting phase in TBLG appears near the first magic angle ($\approx 1.08^{\circ}$) on the hole-doping side ($n < 1$), where the chemical potential is close to a van Hove singularity. The superconducting transition temperature is $T_c \approx 1.7$ K with a renormalized electron bandwidth of about 10 meV.[1] This was observed near a correlated insulating state at half-filling ($n = 0.5$). It is believed that the superconductivity might be mediated by the associated antiferromagnetic quantum critical fluctuations.[33–37] Many theoretical efforts[32–73] have been devoted to understanding the effective low-energy models,[37–48] the nature of the insulating state,[32,33,37–42,49–54] and the gap symmetry of the superconducting phases,[33,35–37,37,47,48,53–61] leading to the proposals of d + id-wave,[33–37,47,48,54–56] p + ip-wave,[47,52,57] nodal s-wave,[53,59] f-wave,[60] and even mixed gap symmetries.[58,61] The nature of the superconducting phases is a subject of heated debate.

The properties of the superconducting TBLG remind us of some of the features of heavy fermion superconductors like $CeCu_2Si_2$.[74,75] In $CeCu_2Si_2$, superconductivity is also mediated by magnetic quantum critical fluctuations, with $T_c \approx 0.6$ K and a heavy electron band of the width of a few meV, similar to those of TBLG. For decades, superconductivity in $CeCu_2Si_2$ has been believed to be a d-wave,[75–77] but recent refined experiments have revealed two nodeless gaps.[78,79] It was pointed out that such a gap structure may be the result of the strong interband quantum critical pairing interaction between coexisting electron and hole Fermi surfaces in $CeCu_2Si_2$.[80] Since the low-energy effective model of TBLG may also have two bands,[37,38] we explore here the possibility of multiple superconducting gaps and study the detailed gap structures taking into account both intra- and interband pairing interactions. For this purpose, we adopt the strong-coupling Eliashberg approach and consider the magnetic quantum critical fluctuations as the candidate pairing glues.[80–89] In comparison with the experiment, we find the most plausible gap symmetry to be a nodeless $s^{\pm}$-wave in the observed range of

*Project supported by the National Key R&D Program of China (Grant No. 2017YFA0303103), the National Natural Science Foundation of China (Grant Nos. 11774401 and 11522435), the State Key Development Program for Basic Research of China (Grant No. 2015CB921303), the Strategic Priority Research Program (B) of the Chinese Academy of Sciences (Grant No. XDB07020200), and the Youth Innovation Promotion Association of the Chinese Academy of Sciences.

†Corresponding author. E-mail: yifeng@iphy.ac.cn

© 2019 Chinese Physical Society and IOP Publishing Ltd 

superconductivity. Moreover, when projected into the valley basis, we obtain f-wave pairing in the valley-singlet component and interesting topological features in the valley-triplet component. Our work highlights the multi-gap nature of the superconductivity in TBLG and the key importance of interband quantum critical pairing interaction. This suggests that TBLG might belong to the same class of unconventional superconductivity as iron-pnictide, electron-doped cuprate, and some heavy fermion superconductors.

Our low-energy effective model is constructed with one $p_x$-like and one $p_y$-like Wannier orbital on each site of the honeycomb Moiré superlattice,[38,43] as schematically illustrated in Fig. 1(b). The resulting four-orbital model describes the four low-energy bands separated by two gaps of about 50 meV from other bands.[16] At the first magic angle, the lattice constant is $a \approx 134$ Å. The mini-Brillouin zone of the superlattice is greatly reduced, as shown in Fig. 1(c). Following Refs. [38] and [43], we adopt the following effective model:

$$H = H_0 + H_1 + H_2. \tag{1}$$

The first term gives the main feature of valley degenerate valence and conduction bands and can be expressed as

$$H_0 = \sum_{\langle\langle i,j\rangle\rangle^{(4)}} t_{ij} \boldsymbol{c}_i^{\dagger} \cdot \boldsymbol{c}_j - \mu \sum_i \boldsymbol{c}_i^{\dagger} \cdot \boldsymbol{c}_i, \tag{2}$$

where $i, j$ denote the sites, $\mu$ is the chemical potential which is responsible for doping away from the Fermi level, and $\boldsymbol{c}_i = (c_{ix}, c_{iy})^{\mathrm{T}}$. In this term, only the hoppings between the same $p_x$ or $p_y$ orbitals are considered and $t_{ij}$ takes the value of $t_1, t_2, t_3, t_4$ depending on the distance between the $i$ and $j$ sites. We consider hoppings up to the fourth nearest neighbor. The second term lifts the degeneracy of the $K$ and $K'$ valleys and

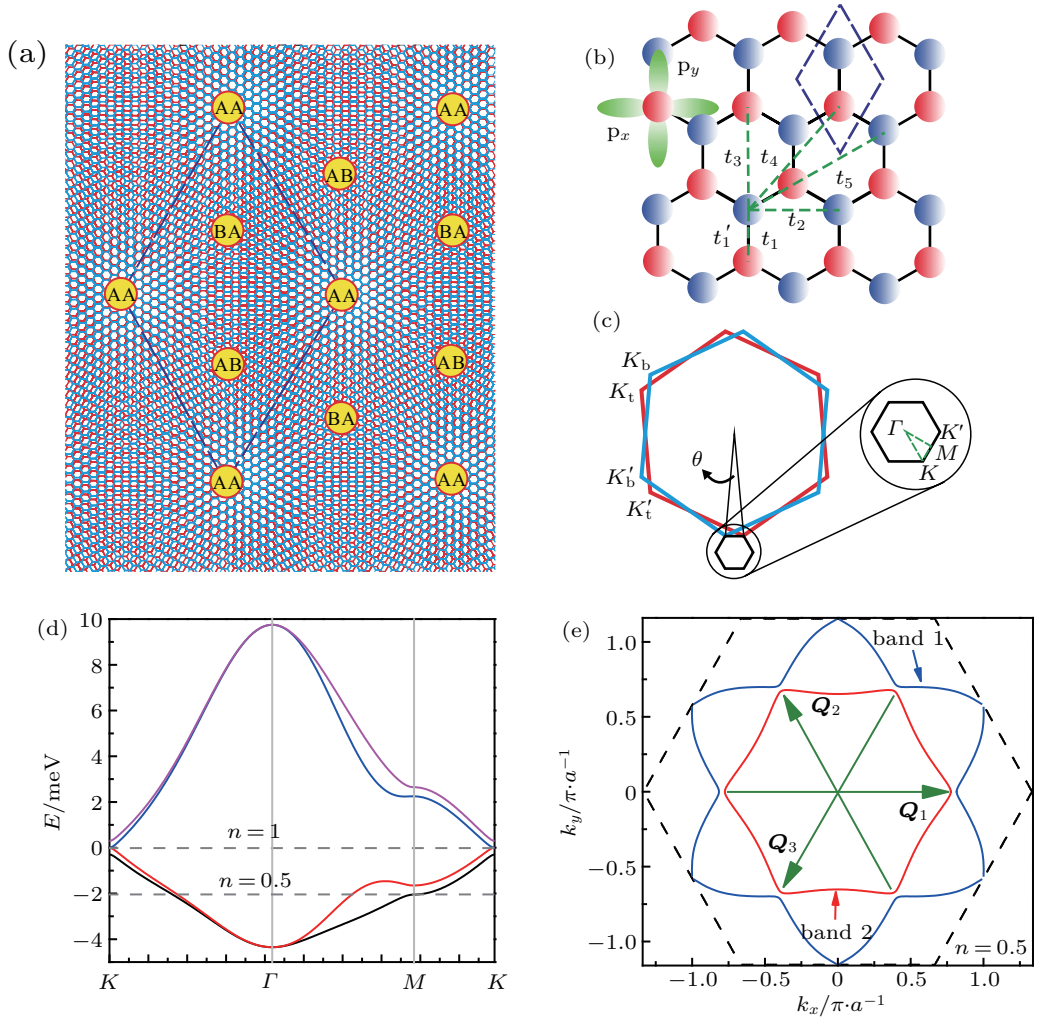



**Fig. 1.** (a) Illustration of the Moiré superlattice in TBLG with small twisted angle. (b) The honeycomb lattice for the tight-binding model used in this work. The $p_{x/y}$-like Wannier orbitals and the hopping parameters are labeled in the figure. In both (a) and (b), the regions enclosed by dashed lines represent a single super unit cell. (c) Illustration of the mini-Brillouin zone of TBLG. $K_t$ and $K_t'$ ($K_b$ and $K_b'$) represent the two inequivalent valleys of the top (bottom) graphene layer. $K$ and $K'$ represent the two inequivalent valleys of TBLG. $\Gamma$ and $M$ are the center and middle points of the $K$–$K'$ line of the mini-Brillouin zone. (d) Effective low-energy band structures along the high symmetry lines in the mini-Brillouin zone. The dashed lines denote the Fermi energy for $n = 0.5$ (half-filling) and 1, where $n$ is one fourth of the total occupation number. $n < 1$ is at the hole-doping side. (e) Typical Fermi surfaces taken at $n = 0.5$, where the two lower bands are half filled. $\boldsymbol{Q}_1$, $\boldsymbol{Q}_2$, and $\boldsymbol{Q}_3$ are the three nesting vectors used in our calculations.

can be written as

$$H_1 = t_5 \sum_{\langle i,j\rangle^{(5)}} \left[ (c_i^\dagger \times c_j)_z + \text{H.c.} \right], \tag{3}$$

where the fifth neighbor hopping between the $p_x$ and $p_y$ orbitals is included. The last term including the nearest neighbor hopping $t_1'$ is

$$H_2 = t_1' \sum_{\langle i,j\rangle} \left[ c_i^\dagger \cdot e_{ij}^{\parallel} e_{ij}^{\parallel} \cdot c_j - c_i^\dagger \cdot e_{ij}^{\perp} e_{ij}^{\perp} \cdot c_j + \text{H.c.} \right], \tag{4}$$

where $e_{ij}^{\parallel}$ and $e_{ij}^{\perp}$ denote the in-plane unit vectors in the directions parallel and perpendicular to the nearest-neighbor bond, respectively. This last term accounts for the hybridization between two valleys and generates a finite Dirac mass at $K$ and $K'$ points.[38] The parameters are chosen such that the bandwidth is of the order of 10 meV and the doping level for half-filling of the two lower bands ($n = 0.5$) is close to the van Hove singularity. Specifically, we adopt the values $t_1 = 2$ meV, $t_2 = 0.3$ meV, $t_3 = 0.05$ meV, $t_4 = 0.15$ meV, $t_5 = 0.12$ meV, and $t_1' = 0.1$ meV. We have ignored the spin–orbit coupling (SOC) which is only $\sim 1\,\mu$eV in graphene and much smaller than the energy scale considered here.[90,91] Figure 1(d) plots the calculated band structures along high symmetry lines of the mini-Brillouin zone. The band structures at $K$ suggest the coexistence of massless and massive Dirac fermions, consistent with both symmetry analysis[38] and quantum oscillation experiment.[1] The Fermi surfaces are nested near the van Hove singularity, as depicted in Fig. 1(e) with the nesting wave vectors $\boldsymbol{Q}_1 = 4\pi/3a(1,0)$, $\boldsymbol{Q}_2 = 4\pi/3a(-1/2, \sqrt{3}/2)$, and $\boldsymbol{Q}_3 = 4\pi/3a(-1/2, -\sqrt{3}/2)$. A Lifshitz transition occurs when the chemical potential is tuned across the van Hove point.

To study the pairing symmetry of superconductivity, we apply the strong-coupling Eliashberg theory and consider two separated Fermi surfaces. The interband (finite momentum) pairing is ignored due to the absence of Fermi surface overlap.[80] Near $T_c$, the linearized Eliashberg equations can be written as

$$\begin{aligned} \lambda \phi_\mu(\boldsymbol{k}, \mathrm{i}\omega_n) = & -\pi T \sum_{\nu,m} \oint_{\mathrm{FS}_\nu} \mathrm{d}k_\parallel' \phi_\nu(\boldsymbol{k}', \mathrm{i}\omega_m) \\ & \times \frac{V^{\mu\nu}(\boldsymbol{k}-\boldsymbol{k}', \mathrm{i}\omega_n - \mathrm{i}\omega_m)}{(2\pi)^2 v_{\boldsymbol{k}_\mathrm{F}'} |\omega_m Z_\nu(\boldsymbol{k}', \mathrm{i}\omega_m)|}, \end{aligned} \tag{5}$$

with

$$\begin{aligned} Z_\mu(\boldsymbol{k}, \mathrm{i}\omega_n) = & 1 + \frac{\pi T}{\omega_n} \sum_{\nu,m} \oint_{\mathrm{FS}_\nu} \mathrm{d}k_\parallel' \mathrm{sgn}(\omega_m) \\ & \times \frac{V^{\mu\nu}(\boldsymbol{k}-\boldsymbol{k}', \mathrm{i}\omega_n - \mathrm{i}\omega_m)}{(2\pi)^2 v_{\boldsymbol{k}_\mathrm{F}'}}, \end{aligned} \tag{6}$$

where $\mu$ and $\nu$ are the band indices, $\omega_n$ is the fermionic Matsubara frequency, $Z_\mu(\boldsymbol{k}, \mathrm{i}\omega_n)$ is the renormalization function, and $\phi_\mu(\boldsymbol{k}, \mathrm{i}\omega_n)$ is related to the gap function through $\phi_\mu(\boldsymbol{k}, \mathrm{i}\omega_n) = Z_\mu(\boldsymbol{k}, \mathrm{i}\omega_n)\Delta_\mu(\boldsymbol{k}, \mathrm{i}\omega_n)$. $V^{\mu\nu}(\boldsymbol{k}-\boldsymbol{k}', \mathrm{i}\omega_n - \mathrm{i}\omega_m)$ represents the intra- or interband scattering of the Cooper pairs. This is an eigenvalue equation and each of its eigen solutions corresponds to a candidate pairing channel. The superconducting symmetry is determined by the leading channel with the largest eigenvalue $\lambda$ at $T_c$. For quantum critical superconductivity, the pairing interactions take the phenomenological form[80,81]

$$V^{\mu\nu}(\boldsymbol{q}, \mathrm{i}\nu_n) = \frac{V_0^{\mu\nu}}{1 + \xi^2(\boldsymbol{q}-\boldsymbol{Q})^2 + |\nu_n|/\omega_{\mathrm{sf}}}, \tag{7}$$

where $\xi$ is the correlation length, $\boldsymbol{Q}$ is the antiferromagnetic wave vector, and $\omega_{\mathrm{sf}}$ is the characteristic energy of the quantum critical fluctuations. The values of $\xi$ and $\omega_{\mathrm{sf}}$ are chosen such that the effective magnetic Fermi energy, $\Gamma_{\mathrm{sf}} = \omega_{\mathrm{sf}}(\xi/a)^2 = 4.3$ meV, is approximately equal to the bandwidth of the two lower bands. $V_0^{\mu\nu}$ are free parameters to be determined experimentally. The resulting gap structures only depend on the relative strengths $r_{11} = V_0^{11}/V_0^{22}$ and $r_{12} = V_0^{12}/V_0^{22}$, while their absolute values play no essential role.

To solve the Eliashberg equations, we further approximate $\Delta_\mu(\boldsymbol{k}, \mathrm{i}\omega_n) = \Delta_\mu(\boldsymbol{k}, \mathrm{i}\pi T_c)$ and $Z_\mu(\boldsymbol{k}, \mathrm{i}\omega_n) = Z_\mu(\boldsymbol{k}, i\pi T_c)$ and use 2048 Matsubara frequencies and $240 \times 240$ $\boldsymbol{k}$-meshes in the mini-Brillouin zone. Typical solutions of the eigenvalue equations are plotted in Fig. 2. The leading solution is a spin-singlet state with nodeless $s^{\pm}$ or doubly degenerate d-wave gap symmetry. This may be understood by recalling that the superlattice has a $D_3$ symmetry group with two one-dimensional and one two-dimensional irreducible representations. The $s^{\pm}$-wave and degenerate d-wave solutions correspond to the $A_1 : 1$, $k_x^2 + k_y^2, \ldots$ and $E : (k_x, k_y)$, $(k_x^2 - k_y^2, k_x k_y)$ representations, respectively. A degenerate p-wave solution is also allowed in the $E$ representation but never becomes dominant in the relevant parameter range. Figure 2(a) shows the four leading values of $\lambda$ with varying $r_{12}$ at fixed $r_{11} = 1.0$. For small $r_{12}$, the d-wave solutions dominate, indicating that the intraband interaction favors d-wave superconductivity on both Fermi surfaces. Since $d_{xy}$ and $d_{x^2-y^2}$ are degenerate, the true gap function here is their linear combination, yielding a chiral d + id-wave pairing symmetry.[37,54] While for large $r_{12} \gtrsim 1.2$, the leading solution is nodeless $s^{\pm}$-wave, induced by a relatively strong interband interaction, as is in pnictide or some heavy fermion superconductors.[80,92,93] A nodal s-wave solution never wins out in the whole parameter range. Figure 2(b) plots the leading eigenvalues at fixed $r_{12} = 1.1$. With increasing $r_{11}$, the dominant d and nodeless $s^{\pm}$-wave solutions exhibit opposite tendencies, reflecting their different physical origins owing to the intra- and inter-band quantum critical pairing interactions, respectively. The momentum distributions of the two solutions are plotted in Figs. 2(c)–2(e). Although the $d_{xy}$ and $d_{x^2-y^2}$ components have nodes, the combined d + id solution is fully gapped. Therefore, both leading solutions are nodeless and may be hard to distinguish in the scanning tunneling experiment.

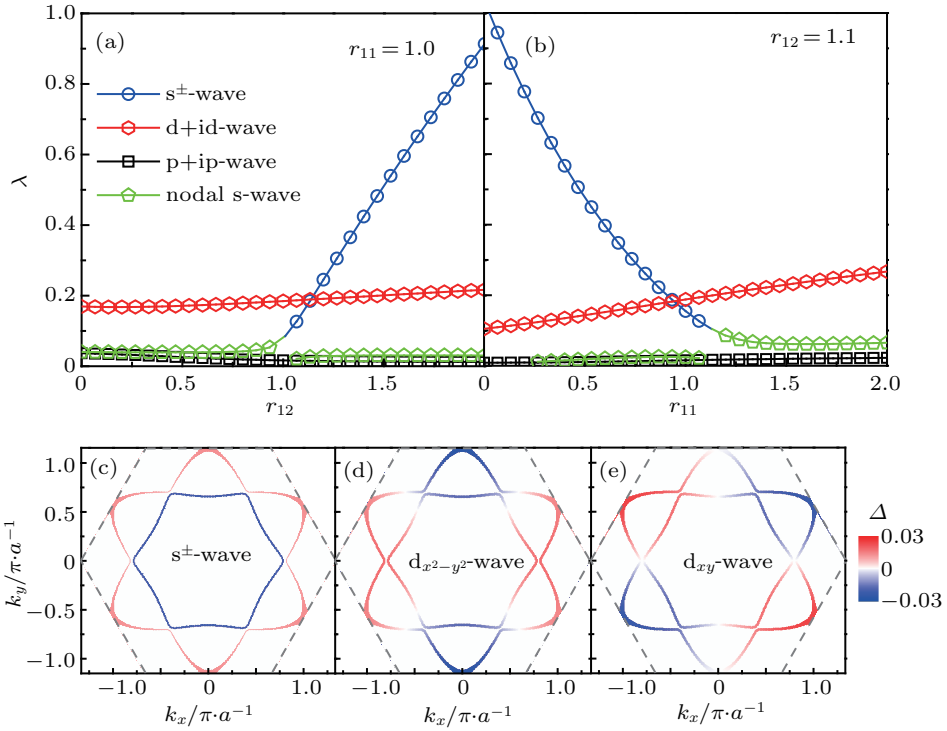



**Fig. 2.** Evolution of the eigenvalues $\lambda$ of four leading solutions with (a) $r_{12}$ for fixed $r_{11}=1.0$ and (b) $r_{11}$ for fixed $r_{12}=1.1$. (c)–(e) The gap distributions on the Fermi surfaces for a typical nodeless s$^{\pm}$-wave solution and the degenerate $d_{x^2-y^2}$ and $d_{xy}$-wave solutions, respectively. We take as an example the results at $n=0.5$.

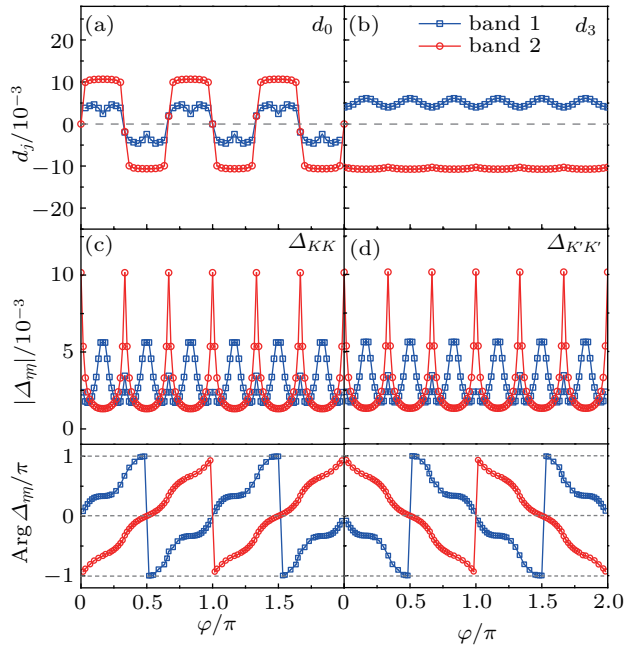



**Fig. 3.** Variation of the gap functions in the valley space with the azimuthal angle $\varphi$, showing (a) the valley-singlet component $d_0$, (b) the valley-triplet component $d_3$, (c) $\Delta_{KK}=-d_1+\mathrm{i}d_2$, and (d) $\Delta_{K'K'}=d_1+\mathrm{i}d_2$ for a typical nodeless s$^{\pm}$-wave solution of the band basis. The upper and lower panels of (c) and (d) plot the magnitude and argument of the two intravalley components, respectively.

While these solutions look simple, they contain certain topological features in the valley space. This may be analyzed considering $\Delta_{\eta\eta'}(\boldsymbol{k})=\sum_{\mu}a_{\eta\mu}(\boldsymbol{k})a_{\eta'\mu}(-\boldsymbol{k})\Delta_{\mu}(\boldsymbol{k})$, under a unitary transformation from band ($\mu$) to valley ($\eta$) bases, $c_{\eta\sigma}(\boldsymbol{k})=\sum_{\mu}a_{\eta\mu}(\boldsymbol{k})c_{\mu\sigma}(\boldsymbol{k})$, where $a_{\eta\mu}(\boldsymbol{k})$ are coefficients of the transformation, $c_{\eta\sigma}(\boldsymbol{k})$ and $c_{\mu\sigma}(\boldsymbol{k})$ are the electron annihilation operators in valley and band spaces. The resulting gap function can be quite generally decomposed into the valley-singlet and triplet components through $\Delta_{\eta\eta'}(\boldsymbol{k})=\sum_j[d_j(\boldsymbol{k})\tau_j\mathrm{i}\tau_2]_{\eta\eta'}$, where $\tau_j$ are the unit matrix for $j=0$ and the Pauli matrices for $j=1,2,3$. The magnitudes of $d_0$ and $\boldsymbol{d}=(d_1,d_2,d_3)$ represent the relative importance of the valley-singlet and triplet contributions. Figure 3 plots the distribution of $d_j(\boldsymbol{k})$ on the Fermi surfaces for a typical solution of nodeless s$^{\pm}$-wave as a function of the azimuthal angle $\varphi$. For spin-singlet pairing, the valley-singlet (triplet) requires odd (even) gap symmetry in the momentum space due to the Pauli principle. As shown in Fig. 3(a), $d_0$ indeed is an odd function in the momentum space. In particular, it has the same sign on both Fermi surfaces at the same azimuthal angle but the overall $\varphi$-dependence exhibits an f-wave manner. Thus the nodeless s$^{\pm}$-wave solution in the band basis contains a valley-singlet f-wave component. The angle dependence of the valley-triplet component is analyzed in Figs. 3(b)–3(d). Quite unexpectedly, while $d_3(\boldsymbol{k})$ is real and varies only slightly with momentum on both Fermi surfaces, $d_1(\boldsymbol{k})$ and $d_2(\boldsymbol{k})$ that correspond to intravalley pairing exhibit unusual topological characters. To see this, we introduce the gap functions on each valley individually, $\Delta_{KK}=-d_1+\mathrm{i}d_2$ and $\Delta_{K'K'}=d_1+\mathrm{i}d_2$, and plot the angle dependence of their amplitudes and phases in Figs. 3(c) and 3(d). A phase change of $4\pi$ or $-4\pi$ is revealed as $\varphi$ varies from 0 to $2\pi$, which is a characteristic feature of topological superconductor with time reversal symmetry.[94] We thus conclude that the valley-triplet com-

ponent has d ± id-wave symmetry in the momentum space. We should note that the existence of $\Delta_{KK}$ and $\Delta_{K'K'}$ is associated with the presumption of valley hybridization in our model Hamiltonian.[38] The relative importance of different valley components may be tuned by experimental manipulation of the valley degree of freedom.[95,96] Absent valley hybridization, the gap function becomes topologically trivial. A similar analysis may be applied to the d + id-wave solution in the band basis (not shown), where the $d_3$ and $d_1 + \mathrm{i}d_2$ components exhibit the phase change of $-4\pi$ and $-8\pi$, respectively, implying its topological nature as chiral superconductivity.[94]

Our results are summarized in Fig. 4(a) on a generic phase diagram with $r_{11}$ and $r_{12}$ as tuning parameters. There are two regions governed by the nodeless $s^{\pm}$-wave for large $r_{12}$ and the d + id-wave for small $r_{12}$. The overall phase boundary is only slightly shifted for different doping levels as shown in Fig. 4(b). Although an exact estimate of the relative importance of the intra- and inter-band quantum critical pairing interactions is not possible at this stage, some preliminary argument might still be made by considering $V_0^{\mu\nu} \propto \mathrm{Re}\chi^{\mu\nu}(\boldsymbol{Q})$, where $\chi^{\mu\nu}(\boldsymbol{Q})$ is the static spin susceptibility at the ordering wave vector $\boldsymbol{Q}$ and may be estimated under the first order approximation using the Lindhard function

$$\chi^{\mu\nu}(\boldsymbol{q}) = \sum_{\boldsymbol{k}} \frac{f_{\mathrm{FD}}(\varepsilon_{\mu\boldsymbol{k}}) - f_{\mathrm{FD}}(\varepsilon_{\nu,\boldsymbol{k}+\boldsymbol{q}})}{\varepsilon_{\nu,\boldsymbol{k}+\boldsymbol{q}} - \varepsilon_{\mu\boldsymbol{k}} + \mathrm{i}\delta}, \tag{8}$$

where $f_{\mathrm{FD}}$ is the Fermi–Dirac distribution function and $\varepsilon_{\mu\boldsymbol{k}}$ is the dispersion of the $\mu$-th band. Taking $n = 0.5$ once again as an example, we plot in Fig. 4(c) the real part of $\chi(\boldsymbol{q}) = \sum_{\mu\nu}\chi^{\mu\nu}(\boldsymbol{q})$ as a function of $\boldsymbol{q}$. As expected, $\mathrm{Re}\chi(\boldsymbol{q})$ reaches maximum when $\boldsymbol{q}$ approaches the nesting wave vectors ($\boldsymbol{Q}_1$, $\boldsymbol{Q}_2$, $\boldsymbol{Q}_3$) at the corners of the mini-Brillouin zone. The corresponding $r_{11}$ and $r_{12}$ can also be estimated and plotted in Fig. 4(d) for generic $n$. A direct comparison with the phase diagram in Fig. 4(b) gives the lower shaded area $R_{\mathrm{C}}$ ($0.4 \lesssim n \lesssim 0.6$) in which the nodeless $s^{\pm}$-wave solution dominates. Experimentally, superconductivity was observed in the upper shaded area labeled as $R_{\mathrm{E}}$. Their overlap implies that nodeless $s^{\pm}$-wave is the most plausible gap symmetry for the superconducting TBLG near half-filling on the hole-doping side.

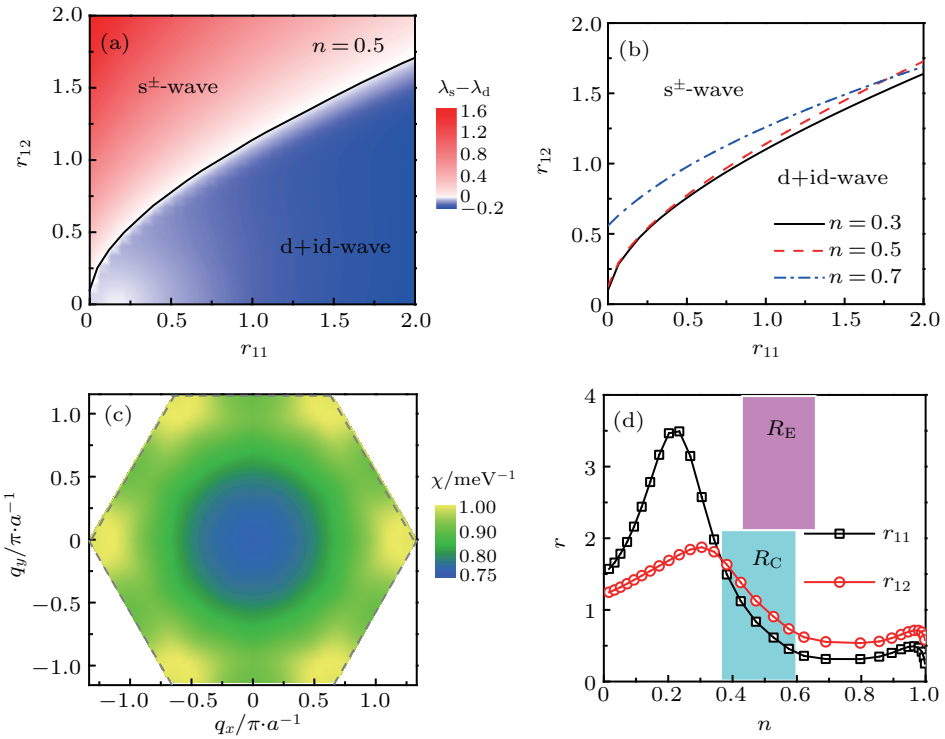



**Fig. 4.** (a) A typical theoretical phase diagram taken with $n = 0.5$. The color is calibrated by the difference between the eigenvalues of the nodeless $s^{\pm}$ and d + id-wave solutions. The solid line marks the boundary of the two phases. (b) Variation of the phase boundary for different doping levels, showing only slight change with $n$. (c) The total spin susceptibility $\chi(\boldsymbol{q})$ evaluated from the Lindhard function, showing maxima at nesting wave vectors. (d) Variation of the estimated $r_{11}$ and $r_{12}$ as a function of the doping level. The shaded area $R_{\mathrm{C}}$ denotes the range where the nodeless $s^{\pm}$-wave becomes dominant, while the shaded area $R_{\mathrm{E}}$ marks the region of superconductivity observed in experiment. The insulating phase (not indicated) is a very narrow region near half-filling within $R_{\mathrm{E}}$.

Our prediction of the nodeless $s^{\pm}$-wave pairing symmetry is deduced from an effective low-energy four-band model with quantum critical pairing interactions and two coexisting Fermi surfaces due to valley hybridization. In previous studies,[33–37,47,48,54–56] a d + id-wave solution was often obtained without considering the presence of strong interband interaction. Absent valley hybridization, p + ip[47,52,57] or nodal s-wave solutions[53,59] have also been proposed depending on

the topology of the Fermi surfaces. On the other hand, a more sophisticated analysis using the functional renormalization group (fRG) was shown to yield an f-wave solution.[60] Actually, this latter work might be consistent with the valley-singlet component in our nodeless $s^{\pm}$-wave solution, as valley hybridization was neglected in the fRG calculations. Further experiments are needed to examine these various possibilities. However, we should note that both the nodeless $s^{\pm}$ and $d+id$-waves are nodeless in the momentum space. Therefore, it might be difficult to distinguish them with the usual scanning tunneling or photoemission spectroscopies. In this respect, phase sensitive measurements using Josephson devices for example[97] have recently been applied to the investigation of 2D topological superconductivity,[98] and Kerr rotation experiments may also be used to detect time reversal symmetry breaking in $d+id$ or $p+ip$-pairings.[99]

To summarize, we explore possible gap symmetry of the superconductivity observed recently in TBLG based on a four-orbital model using the strong-coupling Eliashberg equations with a quantum critical form of the intra- and interband pairing interactions. We find a leading nodeless $s^{\pm}$-wave solution for strong interband interaction and a dominant $d+id$-wave solution originating primarily from the intraband pairing interaction. Both exhibit interesting topological characters in the valley basis. A direct comparison between our theoretical and experimental parameter ranges suggests that the nodeless $s^{\pm}$-wave is the most plausible candidate for the pairing symmetry in superconducting TBLG, different from previous theoretical proposals. The quantum critical nature of the pairing interaction has often been ignored in previous theories. Our work suggests a possible unified description for superconductivity in TBLG and some other correlated superconductors.

## References


[1] Cao Y, Fatemi V, Fang S, Watanabe K, Taniguchi T, Kaxiras E and Jarillo-Herrero P 2018 *Nature* **556** 43
[2] Cao Y, Fatemi V, Demir A, Fang S, Tomarken S L, Luo J Y, Sanchez-Yamagishi J D, Watanabe K, Taniguchi T, Kaxiras E, Ashoori R C and Jarillo-Herrero P 2018 *Nature* **556** 80
[3] Latil S, Meunier V and Henrard L 2007 *Phys. Rev. B* **76** 201402(R)
[4] Morozov S V, Novoselov K S, Katsnelson M I, Schedin F, Elias D C, Jaszczak J A and Geim A K 2008 *Phys. Rev. Lett.* **100** 016602
[5] Mele E J 2010 *Phys. Rev. B* **81** 161405(R)
[6] Bistritzer R and MacDonald A H 2010 *Phys. Rev. B* **81** 245412
[7] Suárez Morell E, Correa J D, Vargas P, Pacheco M and Barticevic Z 2010 *Phys. Rev. B* **82** 121407(R)
[8] Luican A, Li G, Reina A, Kong J, Nair R R, Novoselov K S, Geim A K and Andrei E Y 2011 *Phys. Rev. Lett.* **106** 126802
[9] Moon P and Koshino M 2012 *Phys. Rev. B* **85** 195458
[10] Trambly de Laissardi'ere G, Mayou D and Magaud L 2012 *Phys. Rev. B* **86** 125413
[11] Lopes dos Santos J M B, Peres N M R and Castro Neto A H 2012 *Phys. Rev. B* **86** 155449
[12] Brihuega I, Mallet P, González-Herrero H, Trambly de Laissardi'ere G, Ugeda M M, Magaud L, Gómez-Rodríguez J M, Ynduráin F and Veuillen J Y 2012 *Phys. Rev. Lett.* **109** 196802
[13] González J 2013 *Phys. Rev. B* **88** 125434
[14] Uchida K, Furuya S, Iwata J I and Oshiyama A 2014 *Phys. Rev. B* **90** 155451
[15] Sboychakov A O, Rakhmanov A L, Rozhkov A V and Nori F 2015 *Phys. Rev. B* **92** 075402
[16] Cao Y, Luo J Y, Fatemi V, Fang S, Sanchez-Yamagishi J D, Watanabe K, Taniguchi T, Kaxiras E and Jarillo-Herrero P 2016 *Phys. Rev. Lett.* **117** 116804
[17] Li S Y, Liu K Q, Yin L J, Wang W X, Yan W, Yang X Q, Yang J K, Liu H, Jiang H and He L 2017 *Phys. Rev. B* **96** 155416
[18] Kim K, DaSilva A, Huang S, Fallahazad B, Larentis S, Taniguchi T, Watanabe K, LeRoy B J, MacDonald A H and Tutuc E 2017 *Proc. Natl. Acad. Sci. USA* **114** 3364
[19] Huder L, Artaud A, Quang T L, de Laissardi'ere G T, Jansen A G M, Lapertot G, Chapelier C and Renard V T 2018 *Phys. Rev. Lett.* **120** 156405
[20] Lopes dos Santos J M B, Peres N M R and Castro Neto A H 2007 *Phys. Rev. Lett.* **99** 256802
[21] Mele E J 2011 *Phys. Rev. B* **84** 235439
[22] Yin L J, Qiao J B, Wang W X, Zuo W J, Yan W, Xu R, Dou R F, Nie J C and He L 2015 *Phys. Rev. B* **92** 201408(R)
[23] Fang S and Kaxiras E 2016 *Phys. Rev. B* **93** 235153
[24] Nam N N T and Koshino M 2017 *Phys. Rev. B* **96** 075311
[25] Gonzalez-Arraga L A, Lado J L, Guinea F and San-Jose P 2017 *Phys. Rev. Lett.* **119** 107201
[26] Yan W, Liu M, Dou R F, Meng L, Feng L, Chu Z D, Zhang Y, Liu Z, Nie J C and He L 2012 *Phys. Rev. Lett.* **109** 126801
[27] Li G, Luican A, Lopes dos Santos J M B, Castro Neto A H, Reina A, Kong J and Andrei E Y 2010 *Nat. Phys.* **6** 109
[28] Bistritzer R and MacDonald A H 2011 *Proc. Natl. Acad. Sci. USA* **108** 12233
[29] Trambly de Laissardi'ere G, Mayou D and Magaud L 2010 *Nano Lett.* **10** 804
[30] Ohta T, Robinson J T, Feibelman P J, Bostwick A, Rotenberg E and Beechem T E 2012 *Phys. Rev. Lett.* **109** 186807
[31] Yankowitz M, Jung J, Laksono E, Leconte N, Chittari B L, Watanabe K, Taniguchi T, Adam S, Graf D and Dean C R 2018 *Nature* **557** 404
[32] Kerelsky A, McGilly L, Kennes D M, Xian L, Yankowitz M, Chen S, Watanabe K, Taniguchi T, Hone J, Dean C, Rubio A and Pasupathy A N 2018 arXiv:1812.08776v2 [cond-mat.mes-hall]
[33] Huang T, Zhang L and Ma T 2019 *Sci. Bull.* **64** 310
[34] Xu C and Balents L 2018 *Phys. Rev. Lett.* **121** 087001
[35] Guo H, Zhu X, Feng S and Scalettar R T 2018 *Phys. Rev. B* **97** 235453
[36] Zhang L 2019 *Sci. Bull.* **64** 495
[37] Liu C C, Zhang L D, Chen W Q and Yang F 2018 *Phys. Rev. Lett.* **121** 217001
[38] Yuan N F Q and Fu L 2018 *Phys. Rev. B* **98** 045103
[39] Dodaro J F, Kivelson S A, Schattner Y, Sun X Q and Wang C 2018 *Phys. Rev. B* **98** 075154
[40] Wu X C, Pawlak K A, Jian C M and Xu C 2018 arXiv:1805.06906v1 [cond-mat.str-el]
[41] Ochi M, Koshino M and Kuroki K 2018 *Phys. Rev. B* **98** 081102(R)
[42] Po H C, Zou L, Vishwanath A and Senthil T 2018 *Phys. Rev. X* **8** 031089
[43] Koshino M, Yuan N F Q, Koretsune T, Ochi M, Kuroki K and Fu L 2018 *Phys. Rev. X* **8** 031087
[44] Zou L, Po H C, Vishwanath A and Senthil T 2018 *Phys. Rev. B* **98** 085435
[45] Kang J and Vafek O 2018 *Phys. Rev. X* **8** 031088
[46] Po H C, Zou L, Senthil T and Vishwanath A 2018 arXiv:1808.02482v2 [cond-mat.str-el]
[47] Rademaker L and Mellado P 2018 *Phys. Rev. B* **98** 235158
[48] Venderbos J W F and Fernandes R M 2018 *Phys. Rev. B* **98** 245103
[49] Isobe H, Yuan N F Q and Fu L 2018 *Phys. Rev. X* **8** 041041
[50] Padhi B, Setty C and Phillips P W 2018 *Nano Lett.* **18** 6175
[51] Pizarro J M, Calderón M J and Bascones E 2018 arXiv:1805.07303v1 [cond-mat.str-el]
[52] González J and Stauber T 2019 *Phys. Rev. Lett.* **122** 026801
[53] Sherkunov Y and Betouras J J 2018 *Phys. Rev. B* **98** 205151
[54] Kennes D M, Lischner J and Karrasch C 2018 *Phys. Rev. B* **98** 241407(R)
[55] Lin Y P and Nandkishore R M 2018 *Phys. Rev. B* **98** 214521
[56] Fidrysiak M, Zegrodnik M and Spałek J 2018 *Phys. Rev. B* **98** 085436
[57] Roy B and Juričić V 2019 *Phys. Rev. B* **99** 121407(R)
[58] Su Y and Lin S Z 2018 *Phys. Rev. B* **98** 195101
[59] Ray S and Das T 2019 *Phys. Rev. B* **99** 134515

[60] Tang Q K, Yang L, Wang D, Zhang F C and Wang Q H 2019 *Phys. Rev. B* **99** 094521

[61] You Y Z and Vishwanath A 2019 arXiv:1805.06867v2 [cond-mat.str-el]

[62] Baskaran G 2018 arXiv:1804.00627v1 [cond-mat.supr-con]

[63] Peltonen T J, Ojajärvi R and Heikkilä T T 2018 *Phys. Rev. B* **98** 220504(R)

[64] Irkhin V Y and Skryabin Y N 2018 *JETP Lett.* **107** 651

[65] Zhang Y H, Mao D, Cao Y, Jarillo-Herrero P and Senthil T 2019 *Phys. Rev. B* **99** 075127

[66] Zhu G Y, Xiang T and Zhang G M 2018 arXiv:1806.07535v2 [cond-mat.str-el]

[67] Wu F, MacDonald A H and Martin I 2018 *Phys. Rev. Lett.* **121** 257001

[68] Carr S, Fang S, Jarillo-Herrero P and Kaxiras E 2018 *Phys. Rev. B* **98** 085144

[69] Guinea F and Walet N R 2018 *Proc. Natl. Acad. Sci. USA* **115** 13174

[70] Lian B, Wang Z and Bernevig B A 2019 arXiv:1807.04382v3 [cond-mat.mes-hall]

[71] Song Z, Wang Z, Shi W, Li G, Fang C and Bernevig B A 2018 arXiv:1807.10676v2 [cond-mat.mes-hall]

[72] Laksono E, Leaw J N, Reaves A, Singh M, Wang X, Adam S, Gu X 2018 *Solid State Comm.* **282** 38

[73] Chen L, Li H Z and Han R S 2019 *J. Phys.: Condens. Matter* **31** 065601

[74] Steglich F, Aarts J, Bredl C D, Lieke W, Meschede D, Franz W and Schäfer H 1979 *Phys. Rev. Lett.* **43** 1892

[75] Stockert O, Arndt J, Faulhaber E, Geibel C, Jeevan H S, Kirchner S, Loewenhaupt M, Schmalzl K, Schmidt W, Si Q and Steglich F 2011 *Nat. Phys.* **7** 119

[76] Arndt J, Stockert O, Schmalzl K, Faulhaber E, Jeevan H S, Geibel C, Schmidt W, Loewenhaupt M and Steglich F 2011 *Phys. Rev. Lett.* **106** 246401

[77] Vieyra H A, Oeschler N, Seiro S, Jeevan H S, Geibel C, Parker D and Steglich F 2011 *Phys. Rev. Lett.* **106** 207001

[78] Kittaka S, Aoki Y, Shimura Y, Sakakibara T, Seiro S, Geibel C, Steglich F, Ikeda H and Machia K 2014 *Phys. Rev. Lett.* **112** 067002

[79] Enayat M, Sun Z, Maldonado A, Suderow H, Seiro S, Geibel C, Wirth S, Steglich F and Wahl P 2016 *Phys. Rev. B* **93** 045123

[80] Li Y, Liu M, Fu Z, Chen X, Yang F and Yang Y F 2018 *Phys. Rev. Lett.* **120** 217001

[81] Millis A J, Monien H and Pines D 1990 *Phys. Rev. B* **42** 167

[82] Monthoux P, Balatsky A V and Pines D 1991 *Phys. Rev. Lett.* **67** 3448

[83] Monthoux P and Pines D 1992 *Phys. Rev. Lett.* **69** 961

[84] Millis A J 1992 *Phys. Rev. B* **45** 13047

[85] Monthoux P, Balatsky A V and Pines D 1992 *Phys. Rev. B* **46** 14803

[86] Monthoux P and Pines D 1994 *Phys. Rev. B* **49** 4261

[87] Monthoux P and Lonzarich G G 2002 *Phys. Rev. B* **66** 224504

[88] Dolgov O V, Mazin I I, Parker D and Golubov A A 2009 *Phys. Rev. B* **79** 060502(R)

[89] Yang Y F and Pines D 2014 *Proc. Natl. Acad. Sci. USA* **111** 18178

[90] Min H, Hill J E, Sinitsyn N A, Sahu B R, Kleinman L and MacDonald A H 2006 *Phys. Rev. B* **74** 165310

[91] Yao Y, Ye F, Qi X L, Zhang S C and Fang Z 2007 *Phys. Rev. B* **75** 041401(R)

[92] Bang Y and Stewart G R 2017 *J. Phys.: Condens. Matter* **29** 123003

[93] Kittaka S, Aoki Y, Shimura Y, Sakakibara T, Seiro S, Geibel C, Steglich F, Tsutsumi Y, Ikeda H and Machida K *Phys. Rev. B* **94** 054514

[94] Maeno Y, Kittaka S, Nomura T, Yonezawa S and Ishida K 2012 *J. Phys. Soc. Jpn.* **81** 011009

[95] Xiao D, Yao W and Niu Q 2007 *Phys. Rev. Lett.* **99** 236809

[96] Rycerz A, Tworzydło J and Beenakker C W J 2007 *Nat. Phys.* **3** 172

[97] Van Harlingen D J 1995 *Rev. Mod. Phys.* **67** 515

[98] Charpentier S, Galletti L, Kunakova G, Arpaia R, Song Y, Baghdadi R, Wang S M, Kalaboukhov A, Olsson E, Tafuri F, Golubev D, Linder J, Bauch T and Lombardi F 2017 *Nat. Comm.* **8** 2019

[99] Schemm E R, Baumbach R E, Tobash P H, Ronning F, Bauer E D and Kapitulnik A 2015 *Phys. Rev. B* **91** 140506(R)